







Dipole-forbidden transitions induced by the gradient of optical near fieldsYongkun Chen ¹, Yueming Zhou ^{1,*}, Yijie Liao ¹, Jintai Liang ¹, Xu Zhang,¹ Wei Cao,¹ Min Li ¹,
Marcelo F. Ciappina ^{2,3,4,†} and Peixiang Lu^{1,5}¹*School of Physics and Wuhan National Laboratory for Optoelectronics, Huazhong University of Science and Technology, Wuhan 430074, China*²*Physics Program, Guangdong Technion–Israel Institute of Technology, Shantou, Guangdong 515063, China*³*Technion–Israel Institute of Technology, Haifa, 32000, Israel*⁴*Guangdong Provincial Key Laboratory of Materials and Technologies for Energy Conversion, Guangdong Technion–Israel Institute of Technology, Shantou, Guangdong 515063, China*⁵*Optics Valley Laboratory, Wuhan 430074, China*

(Received 6 May 2022; revised 21 June 2022; accepted 14 October 2022; published 28 October 2022)

The electric-field spatial gradient is a very important property of an optical near-field (ONF). In this study, its effect on the single-photon ionization is theoretically investigated via the three-dimensional time-dependent Schrödinger equation and perturbation theory. The results show that the field gradient can lead to dipole-forbidden transitions, which competes with the usual dipole transition and results in changes of the photoelectron momentum distribution. Additionally, we establish a relationship between the field gradient with the angular distribution of the photoelectrons. Through this mapping, the field gradient can be accurately retrieved. Furthermore, a way for extracting the phase difference between the partial waves with odd and even parity from the photoelectron momentum distribution is proved to be feasible. We find that the Cooper minimum can enhance the effect of the field gradient and thus improves the accuracy of our proposed retrieval procedure. Our results pave the way to exploit atomic structural properties as a probe of the gradient of the ONF.

DOI: [10.1103/PhysRevA.106.043518](https://doi.org/10.1103/PhysRevA.106.043518)**I. INTRODUCTION**

A nanostructure illuminated by a laser field yields to an optical near-field (ONF) in its vicinity. Due to the strong localization and coherent properties of such an ONF, the interaction between this field and matter has a large variety of applications in different areas and techniques, such as surface-enhanced Raman scattering [1–3], photoelectric catalysis [4–7], plasmon-enhanced solar cells [8–10], biosensing [11,12], and so on. In particular, the strong field nonlinear response of the atoms to the ONFs was also extensively studied [13–23]. For example, due to the spatial inhomogeneity and field enhancement of the ONF, the ionized electrons can gain higher energies from the field, attaining the keV regime [15]. Additionally, when the electrons return to the vicinity of the parent ion and recombine with it, high-order harmonics are generated [this is the so-called high-order harmonic generation (HHG) process]. Here, the HHG harmonic cutoff is significantly extended [24–28], reaching up to the carbon K-edge energy, after adequately tuning the driving field and using an adequate target [29]. This property provides a condition for the generation of pulses with picometer spatial and attosecond temporal resolution [30,31]. Meanwhile, because of the high return energies and the modification of the electron

trajectories, the strong-field photoelectron holography in the ONF also undergoes significant changes [32].

To investigate the underlying physics behind the plasmonic-enhanced driven strong-field phenomena, the characterization of the ONFs is necessary [33]. In past years, several techniques were developed to retrieve both the temporal and spatial characteristics of the ONFs. One of the best methods to image the ONFs is the scanning near-field microscopy [34–37]. Here, by using a nanotip, the ONF is far-field mapped, detected, and characterized. Other near-field imaging techniques are based on electron spectroscopy, such as electron-energy-loss spectroscopy, energy-filtered transmission electron microscopy and cathodoluminescence [38–42]. These ways are based on detecting the loss of the kinetic energy of the electrons when they interact with the nanostructure and excite impulsively plasmonic modes, or using the light emitted during the radiative relaxation by detecting the cathodoluminescence. Time-resolved photoemission electron microscopy is also a useful technique which can probe the ONFs with high spatial and temporal resolution [43–46]. In this method, photoelectrons are emitted from a nanostructure illuminated by the far field and imaged by a detector to yield a high-resolution map of the ONFs. In addition, because of the importance of the field enhancement effect, experimental measurements of the local enhanced field strength is one of the basis of nanooptical studies. Through rescattering-based near-field probing techniques, such as the surface-enhanced Raman spectroscopy [47,48], the local enhanced field strength can be obtained. Moreover,

*zhouymhust@hust.edu.cn

†marcelo.ciappina@gtiit.edu.cn

by applying a semiclassical-based model, the local enhanced field strength can be linearly related to the maximum kinetic energy of the electrons emitted from the nanostructure [49–52], providing another indirect way to estimate the enhanced factor.

It should be noted that the local enhanced field gradient is also an important property of the ONFs. However, all previous works were mostly focused on the strong-field regime and determining the influence of the localized field enhancement on the electron dynamics. Thus, little attention was paid to the role of the spatial gradient. In the few-photon region, the effect of the field gradient becomes obvious. For instance, the field spatial gradient can influence the selection rules and enhance dipole-forbidden transitions, which contains not only the quadrupole transition of the target atom itself [53,54], but also additional dipole-forbidden transitions induced by such a spatial gradient. Meanwhile, it was shown that the field gradient of the ONF can intrinsically lead to two-photon absorption [55] and generate second harmonics [56,57]. Furthermore, particularly in the surface-enhanced Raman spectroscopy, the field gradient plays a significant role [3,58–64]. Furthermore, from an engineering perspective, ONF can be an instrumental tool for lithography [65–68]. Coherent light sources in the ultraviolet (UV) to extreme ultraviolet (XUV) spectral range are in high demand nowadays for basic research, material science, biology, and industrial applications, particularly, lithography. Their caveat is a demanding infrastructure for XUV generation and target delivery as well as its low efficiency and low duty cycle. To overcome these problems it was recently demonstrated that the utilization of surface plasmons, also known as plasmonics, as light amplifiers was a feasible alternative. XUV lithography uses light with a wavelength of 13.5 nanometers. This wavelength is more than 14 times shorter than deep ultraviolet light, typically generated from krypton-fluoride (KrF) lasers, that produce light with a wavelength of 248 nm. Although still challenging, the generation of XUV light for lithography using plasmonic-enhanced fields appears to be feasible. To reach this milestone, an accurate and complete characterization, both in time and space, of the ONF be required. Thus, the description of the field gradient in the vicinity of the nanostructure and further techniques to characterize it, appear to be timely both from fundamental as well as engineering viewpoints.

In this paper, we study the single-photon ionization induced by a linearly polarized ONF and demonstrate that the field gradient can be probed by analyzing the photoelectron momentum distribution (PMD). To this end, we numerically solve the three-dimensional time-dependent Schrödinger equation (3D-TDSE) to calculate the PMDs in the ONFs with different frequencies and spatial gradients. The field gradient can induce dipole-forbidden transitions, which compete with the dipole transition and lead to noticeable changes in the PMD. By invoking perturbation theory, we establish a mapping between the field gradient and the angular distribution of the photoelectrons. This relationship paves the way for extracting the field gradient from the PMD. Due to the dipole-forbidden transitions, partial waves with different parity can interfere with each other. We demonstrate that the phase difference between these partial waves can be extracted from the PMD as well. In addition, we show that the Cooper minimum

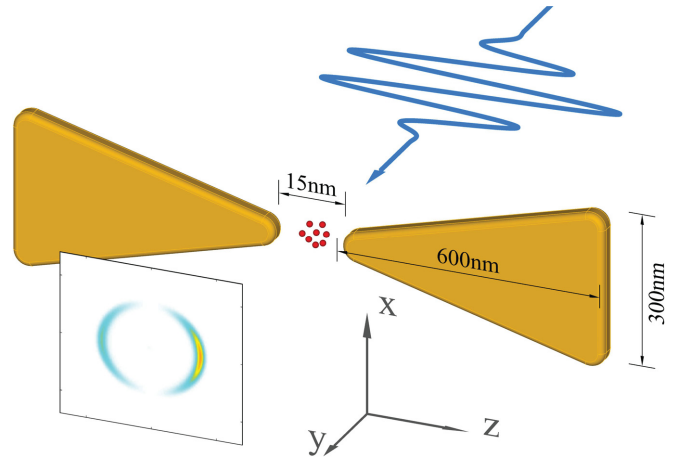


FIG. 1. Schematic representation of the photoelectron momentum distribution driven by a linearly polarized optical near field. An incoming low-intensity laser field illuminates a bow-tie-shaped nanostructure, which yields a much more intense spatially inhomogeneous optical near field. This near field ionizes the electrons from the atoms in the vicinity of the nanostructure and influences the selection rules in the single-photon ionization. The typical parameters of the bow-tie-shaped nanostructure are included.

can be used to enhance the effect of the field gradient and improve the accuracy of its estimation. These techniques provide a tool to probe the field gradient of the ONFs as well as the atomic structural properties.

II. NUMERICAL METHODS

To obtain the PMDs, we numerically solve the 3D-TDSE in the length gauge (atomic units are used unless otherwise stated)

$$i\frac{\partial\Psi(\mathbf{r},t)}{\partial t} = \left(-\frac{1}{2}\nabla^2 + V_a(\mathbf{r}) + V_l(\mathbf{r},t)\right)\Psi(\mathbf{r},t), \quad (1)$$

where $V_l(\mathbf{r},t)$ is the interaction potential between the laser field and the atom and $V_a(\mathbf{r})$ is the model potential of Na that can be written as [69]

$$V_a(\mathbf{r}) = -\frac{1}{r} \left(Z - N + 1 + (N-1) \sum_{p=0}^S c_p r^p e^{-\alpha_p r} \right). \quad (2)$$

Here, these parameters are introduced to reproduce the energy levels of the atom by the Hartree-Fock theory. Their values are given in Ref. [69]. In our simulation, the initial state is the $3s$ state of the Na atom [70–76], with a potential $I_p = 0.1813$ a.u., calculated by using the model potential of Eq. (2). We place the Na atoms between a bow-tie-shaped nanostructure and shine a laser field linearly polarized along the z direction on the nanostructure, as shown in Fig. 1. The ONF, which is spatially inhomogeneous at an atomic scale, i.e., at a subnanometer region, is thus generated at the apex of the nanostructure and interacts with the Na atoms. To exclusively investigate the effect of the field spatial gradient, we do not consider the surface of the nanostructure. Because of the spatially inhomogeneity, the ONF, which is also polarized

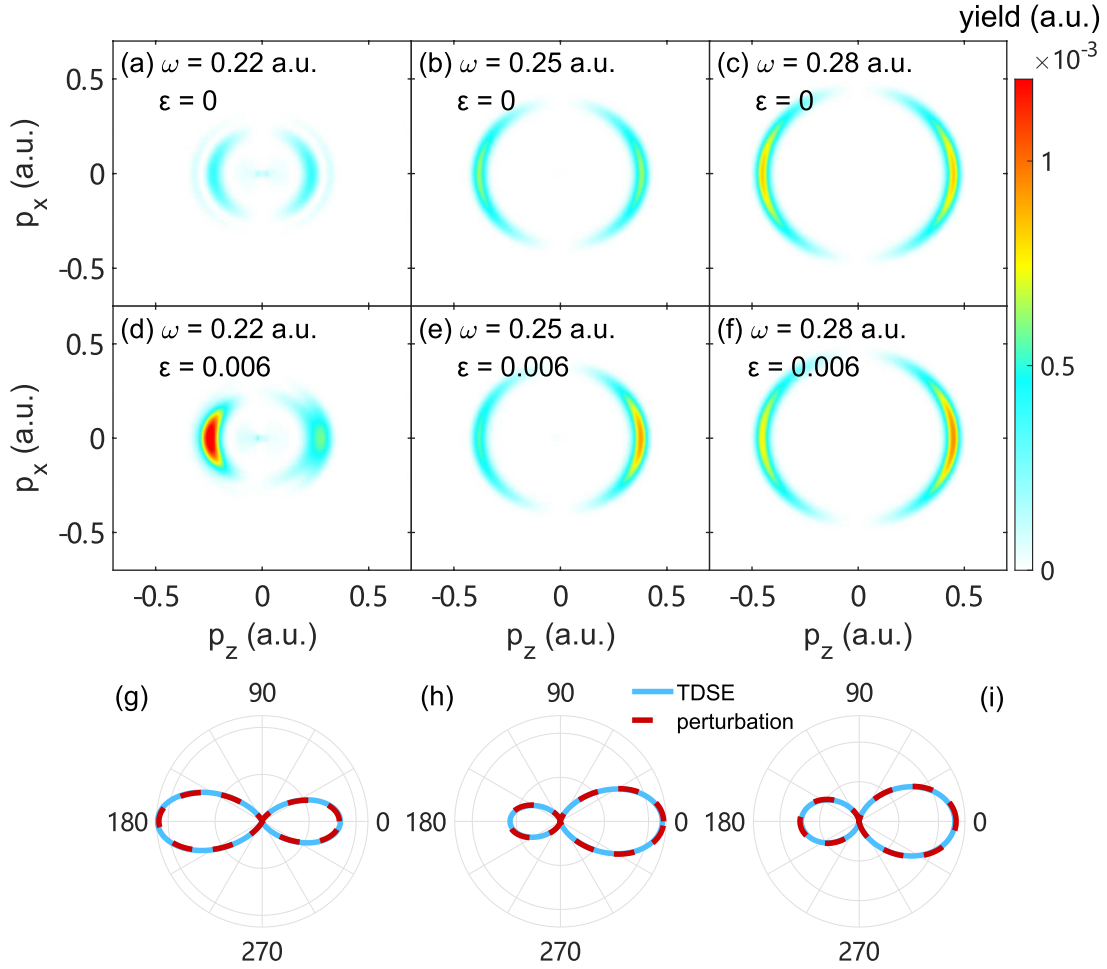


FIG. 2. PMDs for single-photon ionization of Na ($I_p = 0.1813$ a.u.) in a laser field with enhanced intensity $I = 1 \times 10^{12}$ W/cm² (see the text for details). (a)–(c) PMDs in a conventional field ($\varepsilon = 0$) with $\omega = 0.22, 0.25,$ and 0.28 a.u., respectively. (d)–(f) PMDs in an ONF ($\varepsilon = 0.006$) with $\omega = 0.22, 0.25,$ and 0.28 a.u., respectively. (g)–(i) Angular distributions of the PMDs of (d), (e), and (f), respectively. Solid lines: 3D-TDSE; red dashed curves: perturbation theory.

along the z direction, can be expanded as a Taylor series as

$$\mathbf{E}(\mathbf{r}, t) = \mathbf{E}(0, t) + \sum_i \left(\frac{\partial \mathbf{E}(\mathbf{r}, t)}{\partial r_i} \right)_0 + O(r^2). \quad (3)$$

We assume that the field gradient direction is along the polarization direction, thus the laser electric field can be written as

$$\begin{aligned} \mathbf{E}(z, t) &= E(0, t)\hat{z} + \left. \frac{\partial \mathbf{E}(z, t)}{\partial z} \right|_{z=0} \hat{z} \\ &= (1 + 2\varepsilon z)E(0, t)\hat{z} \\ &= (1 + 2\varepsilon z)E_0 f(t) \sin(\omega t)\hat{z}, \end{aligned} \quad (4)$$

where $\left. \frac{\partial \mathbf{E}(z, t)}{\partial z} \right|_{z=0} = 2\varepsilon E(0, t)$ is the field spatial gradient at the position of the atom, with ε the inhomogeneity strength (see, e.g., Ref. [15]). In this way, $V_l(z, t)$ results

$$\begin{aligned} V_l(z, t) &= \int^r \mathbf{dr} \cdot \mathbf{E}(z, t) \\ &= z(1 + \varepsilon z)E_0 f(t) \sin(\omega t). \end{aligned} \quad (5)$$

Here, $f(t)$ is the pulse envelope, which has a $\sin^2(\pi t/T_p)$ form with a duration of $T_p = 16T$ (T is the optical cycle $T = 2\pi/\omega$, where ω is the carrier frequency of the laser field)

and E_0 is the peak strength of the enhanced field at the position of the atom. The plasmonic-enhanced intensity of the laser field is $I = 1 \times 10^{12}$ W/cm² and the propagation direction is along the y direction. Here, the incoming laser intensity is on the order of 10^{10} – 10^{11} W/cm², considering that the plasmonic effect can amplify this field by one or two orders of magnitude. Because of the form of the interaction potential, the transition matrix element of single-photon ionization in the ONF can be written as

$$\begin{aligned} \langle \Psi_{l_f} | z + \varepsilon z^2 | \Psi_{l_i} \rangle &= \langle \Psi_{l_f} | z | \Psi_{l_i} \rangle + \varepsilon \langle \Psi_{l_f} | z^2 | \Psi_{l_i} \rangle \\ &= M_{l_f l_i}^{(1)} + \varepsilon M_{l_f l_i}^{(2)}. \end{aligned} \quad (6)$$

Due to the presence of the term z^2 , dipole-forbidden transitions are now allowed.

It should be noted that the field gradient transition $\langle \Psi_{l_f} | z^2 | \Psi_{l_i} \rangle$ is different from the *conventional* quadrupole transition $\langle \Psi_{l_f} | yz | \Psi_{l_i} \rangle$. The selection rule for the field gradient transition is $\Delta l = 0, \pm 2$ and $\Delta m = 0$, while for quadrupole transition it results in $\Delta l = 0, \pm 2$ and $\Delta m = \pm 1$. It can be seen that the final states of the field gradient transition and the quadrupole transition are different on the magnetic quantum number. This means that the spherical harmonics representing

the angular part of the PMD induced by the field gradient and the quadrupole transitions are orthogonal and are not affected by each other. Therefore, for convenience, we only calculate the field-gradient-induced transition under the dipole approximation and extract the PMDs in the x - z plane (see Fig. 1).

III. RESULTS AND DISCUSSION

We calculate the PMDs for single-photon ionization of a Na atom at different laser frequencies, namely, $\omega = 0.22$, 0.25, and 0.28 a.u. (the corresponding laser wavelengths are $\lambda = 207$, 182, and 162 nm, respectively), by numerically solving the 3D-TDSE, as shown in Fig. 2. Figures 2(a)–2(c) and 2(d)–2(f) show the PMDs in the conventional field ($\varepsilon = 0$) and the ONF ($\varepsilon = 0.006$), respectively. The PMD is plotted as an x - z profile at $p_y = 0$. For the conventional fields, there is an obvious valley in the PMD for $\omega = 0.22$ a.u., as shown in Fig. 2(a). This valley disappears in the case of ONF, as depicted in Fig. 2(d). Meanwhile, the PMDs are symmetric about $p_z = 0$ in the conventional case, while in the ONF the symmetry of the PMDs is broken, and the yield of the ionization increases. The photoelectron yield with negative p_z is higher than that at the positive direction for $\omega = 0.22$ a.u. [Fig. 2(d)]. As the frequency increases to 0.25 [Fig. 2(e)] or 0.28 a.u. [Fig. 2(f)], the yield with the positive p_z becomes higher. This asymmetry is more clearly seen in the angular distributions, as shown in Figs. 2(g)–2(i) (blue solid curves). It can be seen that the asymmetry for $\omega = 0.25$ a.u. [Fig. 2(h)] is stronger than that for $\omega = 0.22$ [Fig. 2(g)] and 0.28 a.u. [Fig. 2(i)].

In single-photon ionization from the $3s$ initial state of Na, the PMD can be expressed as [77]

$$I(\theta, \varphi, \varepsilon) = |\varepsilon A_s Y_0^0(\theta, \varphi) + A_p Y_1^0(\theta, \varphi) + \varepsilon A_d Y_2^0(\theta, \varphi)|^2 = \sum_{n=0}^4 \beta_n(\varepsilon) P_n[\cos(\theta)], \quad (7)$$

where θ is the angle between the polarization axis of the ONF and the direction of the outgoing electron and φ is the azimuth angle. A_s , A_p , and A_d are the transition amplitudes of the s - s , s - p , and s - d channels, respectively. The series expansion in Legendre polynomials P_n extends up to the fourth order and the anisotropy parameters β_n have the following expressions:

$$\beta_0(\varepsilon) = \frac{1}{4\pi} |A_p|^2 + \frac{1}{4\pi} [|A_s|^2 + |A_d|^2] \varepsilon^2, \quad (8a)$$

$$\beta_1(\varepsilon) = \frac{1}{4\pi} \left[2\sqrt{3} |A_s| |A_p| \cos(\phi_s - \phi_p) + \frac{4\sqrt{15}}{5} |A_p| |A_d| \cos(\phi_p - \phi_d) \right] \varepsilon, \quad (8b)$$

$$\beta_2(\varepsilon) = \frac{1}{2\pi} |A_p|^2 + \frac{1}{4\pi} \left[\frac{10}{7} |A_d|^2 + 2\sqrt{5} |A_s| |A_d| \cos(\phi_s - \phi_d) \right] \varepsilon^2, \quad (8c)$$

$$\beta_3(\varepsilon) = \frac{1}{4\pi} \frac{6\sqrt{15}}{5} |A_p| |A_d| \cos(\phi_p - \phi_d) \varepsilon, \quad (8d)$$

$$\beta_4(\varepsilon) = \frac{1}{4\pi} \frac{18}{7} |A_d|^2 \varepsilon^2. \quad (8e)$$

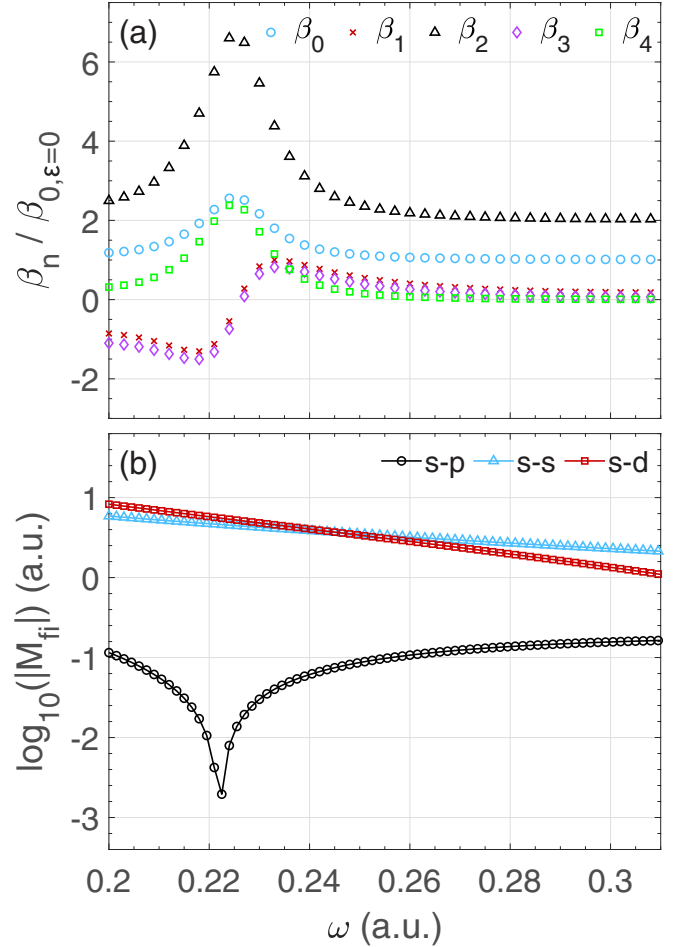


FIG. 3. (a) Anisotropy parameters β_n as a function of the laser frequency ω . Here blue circles: β_0 ; red crosses: β_1 ; black triangles: β_2 ; purple diamonds: β_3 ; and green squares: β_4 . The field gradient parameter is $\varepsilon = 0.006$ and the unit $\beta_{0, \varepsilon=0}$ is the anisotropy parameter of the PMD in the conventional field ($\varepsilon = 0$). (b) Amplitude (logarithmic scale) of the dipole and dipole-forbidden transition channels as a function of the photon energy ω . Black circles: dipole transition s - p channel (conventional field). Gradient field transitions channels: blue triangles: s - s channel and red squares: s - d channel. The Cooper minimum is near $\omega_c = 0.223$ a.u.

Here, within the lowest order of perturbation theory, the transition amplitudes can be written as

$$A_p(E_f) = -i \int dt e^{-i(E_f - I_p)t} E(t) M_{ps}^{(1)}, \quad (9a)$$

$$A_s(E_f) = -i \int dt e^{-i(E_f - I_p)t} E(t) M_{ss}^{(2)}, \quad (9b)$$

$$A_d(E_f) = -i \int dt e^{-i(E_f - I_p)t} E(t) M_{ds}^{(2)}, \quad (9c)$$

where $A_p(E_f)$ is the dipole transition amplitude and $A_s(E_f)$, $A_d(E_f)$ are the amplitudes of the transition (s - s path and s - d path), which only exist in a laser field with a spatial gradient. The angular distributions calculated via the perturbation theory are shown in Figs. 2(g)–2(i) (red dashed curves) and they agree very well with the results obtained from the 3D-TDSE.

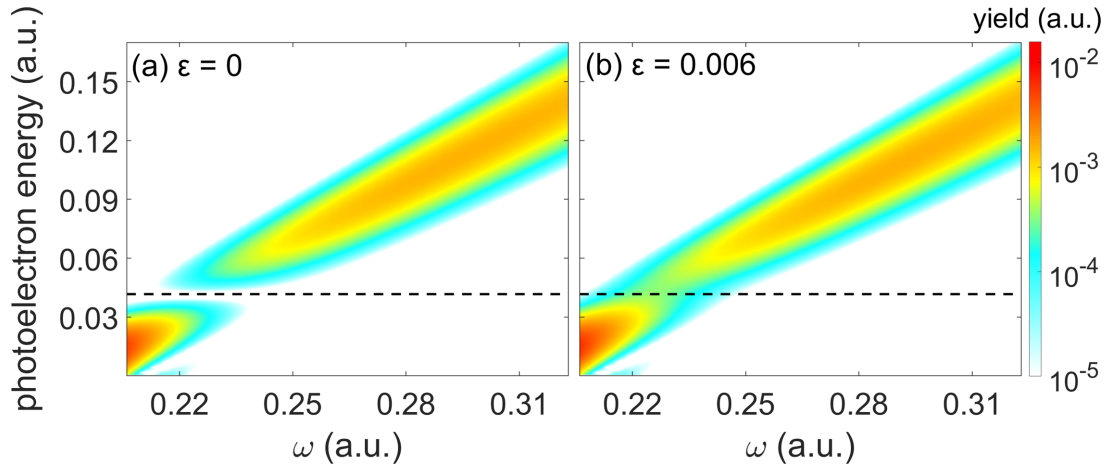


FIG. 4. Photoelectron energy spectra at different laser frequencies ω . (a) $\varepsilon = 0$ and (b) $\varepsilon = 0.006$. The black horizontal dashed line represents the Cooper minimum ($\omega_c - I_p = 0.0417$ a.u.).

The influence of the field gradient is reflected in the competition of the above three transition channels, which leads to changes in the angular distribution of the PMD. Figure 3 displays the variation of the anisotropy parameters β_n and the different transition amplitudes with ω . In Fig. 3(a), we show that β_0 , β_2 , and β_4 have maximal values near $\omega_c = 0.223$ a.u., and β_1 , β_3 change their signs. Similarly, in Fig. 3(b), the s - p channel has a Cooper minimum near ω_c , which is induced by the nodes of the $3s$ initial state radial wave function of the Na atom [78]. This minimum is represented as a narrow valley in the PMD, as shown in Fig. 2(a). Due to the Cooper minimum, the contribution of the s - p channel to the PMD becomes weak, leading to a dominance of the other transition channels (s - s and s - d). This enhances the influence of the field gradient transitions. Therefore, β_0 , β_2 , and β_4 , which are composed of the contributions of the field gradient transitions, reach their maximum values with respect to the gradient-free anisotropy parameter $\beta_{0,\varepsilon=0}$ at ω_c . Meanwhile, the Cooper minimum can result in a phase jump of the s - p channel, which explains why β_1 and β_3 , formed by the interference between the dipole transition and the field gradient transitions, change signs near ω_c . In addition, the asymmetry of the PMD results from the interference between the partial waves with odd and even parity. Thus the phase jump of the p wave can invert the constructive and destructive interference near the photoelectron energy extremes, resulting in the opposite asymmetric form of the PMD on both sides of ω_c , as shown in Figs. 2(d), 2(e) 2(g), and 2(h).

In Fig. 3(b), with the increase of the laser frequency, the contribution of the field gradient transitions decreases gradually. When the laser frequency is around 0.24 a.u., the contributions of the three transition channels are roughly equal, i.e., $M_{ps}^{(1)} \approx \varepsilon M_{ss}^{(2)} \approx \varepsilon M_{ds}^{(2)}$, leading to a strong interference between them. In this frequency region, the ratio of the interference terms β_1 , β_3 in the PMD can reach the maximum. Thus, the asymmetry of the angular distribution is most obvious, as shown in Fig. 2(h). But, as the frequency continues to increase, the contributions of the field gradient transitions to the PMD are much less important than that of the dipole transition and the effect of the field gradient becomes insignificant. Therefore, in the high-frequency region,

β_1 , β_3 , β_4 tend to zero; β_0 tends to $\beta_{0,\varepsilon=0}$; and β_2/β_0 tends to $2/1$, which is the conventional relationship of these anisotropy parameters in single-photon ionization without a field gradient. In Fig. 2, it also can be seen that the enhancement of the ionization yield becomes weaker as the frequency increases. These phenomena are more obvious in Fig. 4, which shows the photoelectron energy spectra at different laser frequencies. In the case of $\varepsilon = 0$, a valley produced by the Cooper minimum can be clearly seen. When the field gradient is turned on, the valley is filled in by the nonzero gradient transition channels. In the high-frequency region, however, there is no significant difference between these two spectra due to the weak effect of the field gradient transitions. In general, by changing the frequency, the competition of the different transition channels can be controlled and the field gradient influence can be amplified, which is beneficial for us to extract useful information from the PMD.

In the following, we discuss an interesting point. Equations (8a)–(8e) reveal a mapping between the anisotropy parameters β_n and the field gradient parameter ε . Figure 5 shows this relationship for different frequencies, calculated by the 3D-TDSE and perturbation theory. We observe an excellent agreement between both approaches. It can be seen that β_0 , β_2 , β_4 are proportional to ε^2 , and β_1 , β_3 , which are only formed by the interference between the dipole and the field gradient transitions, are proportional to ε . Through this mapping, the field spatial gradient can be extracted from the PMD in the ONF. When the laser frequency varies, however, the sensitivity of the PMD to the spatial gradient also changes. Thus, the accuracy of the field gradient estimation procedure results are affected. In Fig. 5(a), it is shown that β_n varies dramatically with ε for the case of $\omega = 0.22$ a.u., which is near the frequency of the Cooper minimum. In this frequency the PMD is very sensitive to the field gradient. A tiny spatial gradient can significantly influence the PMD, e.g., as β_2 doubles at $\varepsilon = 0.004$, it is clear that this small spatial gradient can be probed easily and accurately. As ω increases, the variation of β_n with ε slows down, as shown in Figs. 5(b) and 5(c). When the frequency increases to 0.28 a.u., the field gradient has little influence in the PMD. Even if $\varepsilon = 0.01$, β_0 and β_2 increase to no more than 5%. Thus, in the high-frequency

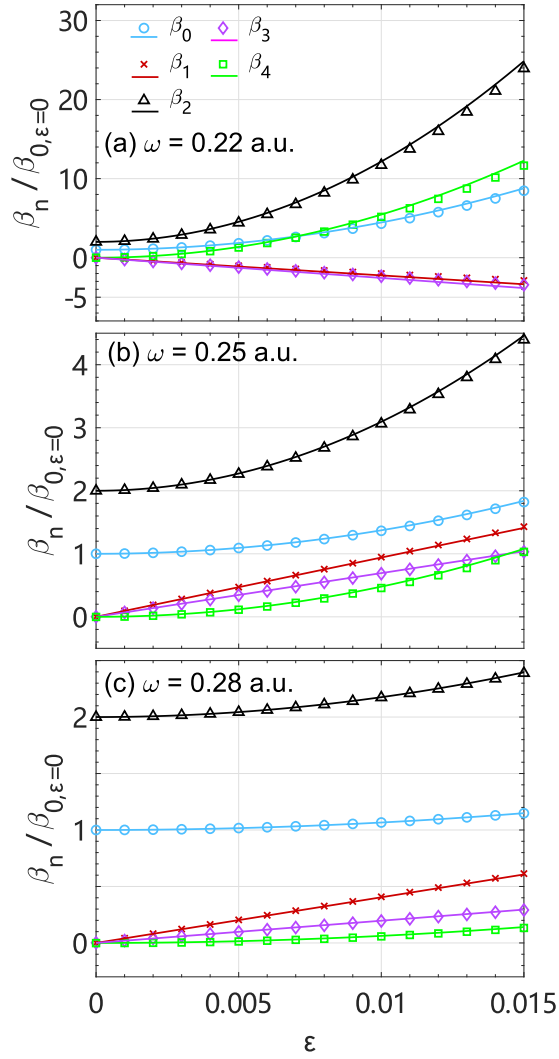


FIG. 5. Dependence of the anisotropy parameters β_n on the field gradient ε . Here open circles: β_0 ; red crosses: β_1 ; black triangles: β_2 ; purple diamond: β_3 ; and green squares: β_4 . The symbols and the solid curves are the results of the TDSE and perturbation theory, respectively. (a) $\omega = 0.22$ a.u., (b) $\omega = 0.25$ a.u., and (c) $\omega = 0.28$ a.u., respectively. The enhanced laser intensity is $I = 1 \times 10^{12}$ W/cm². The unit $\beta_{0, \varepsilon=0}$ is the anisotropy parameter of the PMD in the conventional field ($\varepsilon = 0$) at the respective laser frequencies.

region, the field gradient effect becomes too weak to extract any precise information about it from the photoelectron angular distributions.

To prove the validity of our method, we demonstrate the extraction of the field gradient from the PMDs in an ONF with $\varepsilon = 0.006$, with a assumption that the modulus of the transition amplitudes are known. The results are shown in Fig. 6(a). In the region near the frequency of the Cooper minimum, the extracted result is roughly equal to 0.006, agreeing very well with the set value. When $\omega < \omega_c$, these two results still agree with each other. This is because, even if the region is not near the frequency of the Cooper minimum, the field gradient transitions dominate in the competition between all transitions. Thus, the significant effect of the spatial gradient leads to a high accuracy of the retrieval method. In the high-frequency region, however, the weakening of the field gradient effect

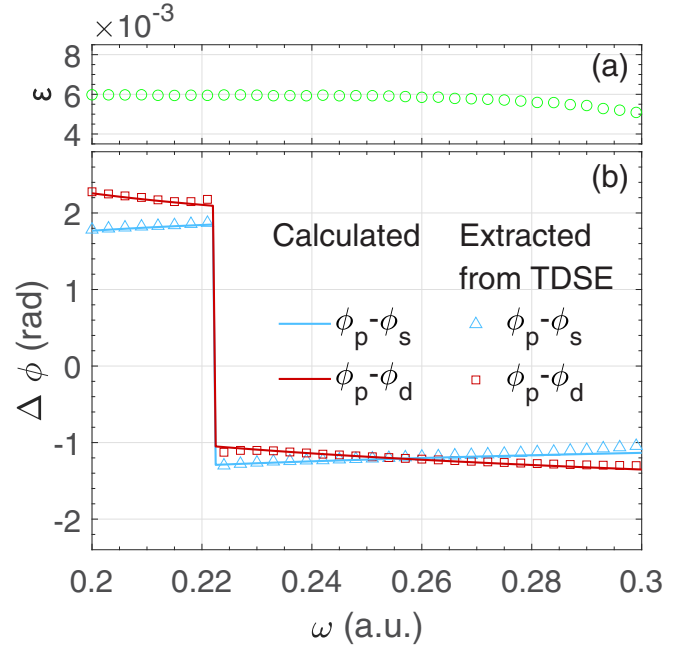


FIG. 6. (a) Field spatial gradient extracted from the PMDs at different photon energies ω . (b) Phase difference of the partial waves with different parity as a function of the photon energy ω . Symbols (squares and triangles): results extracted from the 3D-TDSE calculations. Blue triangles: $\phi_p - \phi_s$. Red squares: $\phi_p - \phi_d$. Solid lines: results obtained from numerically calculations based on the partial wave method. Blue line: $\phi_p - \phi_s$. Red line: $\phi_p - \phi_d$.

reduces the accuracy of the retrieval procedure, resulting in an increase of the error in the extracted result. In addition, we should note the interference between the partial waves with different parity in the PMD. Using this interference effect, the phase difference between them can be extracted, which is an important parameter in the nondipole driven phenomena studies [79,80]. Figure 6(b) shows the phase difference extracted by the 3D-TDSE (open squares and triangles) compared with those calculated using the partial wave method (solid lines) [81]. An excellent agreement can be observed between these two approaches. It can be also seen that these two phase differences have phase jumps of π near ω_c , and their trends with the laser frequency are the opposite. This means that the phases of the partial waves with different angular momentum quantum numbers increase at different rates with the laser frequency. The higher the angular momentum quantum number, the faster the increase rate. As the frequency increases, the phase difference $\phi_p - \phi_s$ has a small error due to the weakening of the field gradient effect. With this demonstration, we prove the feasibility of the extraction procedure based on the anisotropy parameters of the PMD in the ONF and the application of the Cooper minimum in improving the accuracy of the retrieval method. Here, the extracted results are accurate within a certain frequency range. Our approach extends the application of the atomic response in the ONFs, and provides a tool to probe the field gradient and the phase difference between the continuum state wave functions with different parities.

In our theoretical study, we assume that the Na atom is placed at a given position. Experimentally speaking, however,

the atoms are randomly distributed between the bow-tie-shaped nanostructure. Thus, the measured PMD results as an average over the region where the atoms are spread. Furthermore, in laser photoionization, the ionization rate depends on the intensity of the laser field. In the ONF, the field is strongest near the tip of the nanostructure, and thus it has the largest contribution to the measured signal. Therefore, we expect the field gradient extracted from the measured PMD is the one near the tip of the nanostructure.

IV. CONCLUSION

In this paper we study the PMD in single-photon ionization induced by an ONF and demonstrate that the field gradient leads to noticeable variations of the PMD. Through the numerical solution of the 3D-TDSE, the PMD in the ONF can be obtained. The competition between the dipole transitions and the field gradient transitions leads to pronounced changes in the PMD. Through changes in the laser frequency, the influence of the field gradient can be controlled. Within perturbation theory, a mapping between the field gradient and the anisotropy parameters of the PMD is established, which provides a tool to probe the spatial gradient of the ONF. We also verify that the phase difference between the partial waves with

different parity can be extracted from the photoelectron angular distribution, which can be used to probe atomic structural properties. It is shown that the Cooper minimum can increase the proportion of the field gradient transitions in the PMD through reducing the contribution of the dipole transition and improve the accuracy of above-described retrieval procedure. Our method thus provides an alternative feature present in the atomic response driven by an ONF and paves the way for simultaneously detecting the field spatial gradient and atomic structural features.

ACKNOWLEDGMENTS

This work was supported by National Key Research and Development Program of China (Grant No. 2019YFA0308300) and National Natural Science Foundation of China (Grants No. 11874163, and No. 12021004). MFC acknowledges financial support from the Guangdong Province Science and Technology Major Project (Future functional materials under extreme conditions Grant No. 2021B0301030005). The computing work in this paper is supported by the Public Service Platform of High Performance Computing provided by Network and Computing Center of HUST.

-
- [1] M. Moskovits, Surface-enhanced spectroscopy, *Rev. Mod. Phys.* **57**, 783 (1985).
 - [2] K. Kneipp, Y. Wang, H. Kneipp, L. T. Perelman, I. Itzkan, R. R. Dasari, and M. S. Feld, Single Molecule Detection Using Surface-Enhanced Raman Scattering (SERS), *Phys. Rev. Lett.* **78**, 1667 (1997).
 - [3] E. J. Ayars, H. D. Hallen, and C. L. Jahncke, Electric Field Gradient Effects in Raman Spectroscopy, *Phys. Rev. Lett.* **85**, 4180 (2000).
 - [4] A. Fujishima and K. Honda, Electrochemical photolysis of water at a semiconductor electrode, *Nature (London)* **238**, 37 (1972).
 - [5] T. Inoue, A. Fukushima, S. Konishi, and K. Honda, Photoelectrocatalytic reduction of carbon dioxide in aqueous suspensions of semiconductor powders, *Nature (London)* **277**, 637 (1979).
 - [6] K. Maeda, K. Teramura, D. Lu, T. Takata, N. Saito, Y. Inoue, and K. Domen, Photocatalyst releasing hydrogen from water, *Nature (London)* **440**, 295 (2006).
 - [7] E. Kazuma, J. Jung, H. Ueba, M. Trenary, and Y. Kim, Real-space and real-time observation of a plasmon-induced chemical reaction of a single molecule, *Science* **360**, 521 (2018).
 - [8] S. Pillai, K. R. Catchpole, T. Trupke, and M. A. Green, Surface plasmon enhanced silicon solar cells, *J. Appl. Phys.* **101**, 093105 (2007).
 - [9] K. Nakayama, K. Tanabe, and H. A. Atwater, Plasmonic nanoparticle enhanced light absorption in GaAs solar cells, *Appl. Phys. Lett.* **93**, 121904 (2008).
 - [10] K. R. Catchpole and A. Polman, Design principles for particle plasmon enhanced solar cells, *Appl. Phys. Lett.* **93**, 191113 (2008).
 - [11] M. Malmqvist, Biospecific interaction analysis using biosensor technology, *Nature (London)* **361**, 186 (1993).
 - [12] F.-C. Chien and S.-J. Chen, A sensitivity comparison of optical biosensors based on four different surface plasmon resonance modes, *Biosens. Bioelectron.* **20**, 633 (2004).
 - [13] G. Herink, D. R. Solli, M. Gulde, and C. Ropers, Field-driven photoemission from nanostructures quenches the quiver motion, *Nature (London)* **483**, 190 (2012).
 - [14] M. F. Ciappina, J. Biegert, R. Quidant, and M. Lewenstein, High-order-harmonic generation from inhomogeneous fields, *Phys. Rev. A* **85**, 033828 (2012).
 - [15] M. F. Ciappina, J. A. Pérez-Hernández, T. Shaaran, J. Biegert, R. Quidant, and M. Lewenstein, Above-threshold ionization by few-cycle spatially inhomogeneous fields, *Phys. Rev. A* **86**, 023413 (2012).
 - [16] Z. Wang, P. Lan, J. Luo, L. He, Q. Zhang, and P. Lu, Control of electron dynamics with a multicycle two-color spatially inhomogeneous field for efficient single-attosecond-pulse generation, *Phys. Rev. A* **88**, 063838 (2013).
 - [17] L. Ortmann, J. A. Pérez-Hernández, M. F. Ciappina, J. Schötz, A. Chacón, G. Zeraoui, M. F. Kling, L. Roso, M. Lewenstein, and A. S. Landsman, Emergence of a Higher Energy Structure in Strong Field Ionization with Inhomogeneous Electric Fields, *Phys. Rev. Lett.* **119**, 053204 (2017).
 - [18] I. N. Ansari, C. Hofmann, L. Medžišauskas, M. Lewenstein, M. F. Ciappina, and G. Dixit, Controlling polarization of attosecond pulses with plasmonic-enhanced bichromatic counter-rotating circularly polarized fields, *Phys. Rev. A* **103**, 013104 (2021).
 - [19] X.-Y. Wu, H. Liang, X.-S. Kong, Q. Gong, and L.-Y. Peng, Enhancement of high-order harmonic generation in two-dimensional materials by plasmonic fields, *Phys. Rev. A* **103**, 043117 (2021).
 - [20] X.-Z. Gao, A. Landsman, H. Wang, P. Huang, Y. Zhang, B. Wang, Y. Wang, H. Cao, Y. Fu, and L.-W. Pi, Analysis of a

- higher-energy structure in nanotip enhanced fields, *New J. Phys.* **23**, 113017 (2021).
- [21] M. F. Ciappina, J. A. Pérez-Hernández, A. S. Landsman, W. A. Okell, S. Zherebtsov, B. Förg, J. Schötz, L. Seiffert, T. Fennel, T. Shaaran, T. Zimmermann, A. Chacón, R. Guichard, A. Zaïr, J. W. G. Tisch, J. P. Marangos, T. Witting, A. Braun, S. A. Maier, L. Roso *et al.*, Attosecond physics at the nanoscale, *Rep. Prog. Phys.* **80**, 054401 (2017).
- [22] J. Schoetz, Z. Wang, E. Pisanty, M. Lewenstein, M. F. Kling, and M. F. Ciappina, Perspective on petahertz electronics and attosecond nanoscopy, *ACS Photonics* **6**, 3057 (2019).
- [23] S. Kim, T.-I. Jeong, J. Park, M. F. Ciappina, and S. Kim, Recent advances in ultrafast plasmonics: from strong field physics to ultraprecision spectroscopy, *Nanophotonics* **11**, 2393 (2022).
- [24] A. Husakou, S.-J. Im, and J. Herrmann, Theory of plasmon-enhanced high-order harmonic generation in the vicinity of metal nanostructures in noble gases, *Phys. Rev. A* **83**, 043839 (2011).
- [25] T. Shaaran, M. F. Ciappina, R. Guichard, J. A. Pérez-Hernández, L. Roso, M. Arnold, T. Siegel, A. Zaïr, and M. Lewenstein, High-order-harmonic generation by enhanced plasmonic near fields in metal nanoparticles, *Phys. Rev. A* **87**, 041402(R) (2013).
- [26] B. Fetić and D. Milošević, Carrier-envelope-phase control of plasmonic-field enhanced high-order harmonic generation, *J. Mod. Opt.* **60**, 1466 (2013).
- [27] E. Neyra, F. Videla, M. F. Ciappina, J. A. Pérez-Hernández, L. Roso, M. Lewenstein, and G. A. Torchia, High-order harmonic generation driven by inhomogeneous plasmonics fields spatially bounded: influence on the cut-off law, *J. Opt.* **20**, 034002 (2018).
- [28] A. Mandal, P. C. Deshmukh, and K. P. Singh, Controlling high harmonic generation using inhomogeneous two-color driving laser pulse, *Laser Phys.* **31**, 075302 (2021).
- [29] J. A. Pérez-Hernández, M. F. Ciappina, M. Lewenstein, L. Roso, and A. Zaïr, Beyond Carbon *K*-Edge Harmonic Emission using a Spatial and Temporal Synthesized Laser Field, *Phys. Rev. Lett.* **110**, 053001 (2013).
- [30] I. Yavuz, E. A. Bleda, Z. Altun, and T. Topcu, Generation of a broadband XUV continuum in high-order-harmonic generation by spatially inhomogeneous fields, *Phys. Rev. A* **85**, 013416 (2012).
- [31] A. Farmani, S. Sarikhani, and S. Batebi, Behavioral study of high-order harmonics and attosecond pulse generation in a spatially non-homogeneous laser field, *Opt. Commun.* **439**, 47 (2019).
- [32] Y. Chen, Y. Zhou, J. Tan, M. Li, W. Cao, and P. Lu, Photoelectron holography in strong-field tunneling ionization by a spatially inhomogeneous field, *Phys. Rev. A* **104**, 043107 (2021).
- [33] P. Dombi, Z. Pápa, J. Vogelsang, S. V. Yalunin, M. Sivilis, G. Herink, S. Schäfer, P. Groß, C. Ropers, and C. Lienau, Strong-field nano-optics, *Rev. Mod. Phys.* **92**, 025003 (2020).
- [34] D. W. Pohl, W. Denk, and M. Lanz, Optical stethoscopy: Image recording with resolution $\lambda/20$, *Appl. Phys. Lett.* **44**, 651 (1984).
- [35] E. Betzig, J. K. Trautman, T. D. Harris, J. S. Weiner, and R. L. Kostelak, Breaking the diffraction barrier: optical microscopy on a nanometric scale, *Science* **251**, 1468 (1991).
- [36] R. Hillenbrand and F. Keilmann, Complex Optical Constants on a Subwavelength Scale, *Phys. Rev. Lett.* **85**, 3029 (2000).
- [37] J.-J. Greffet and R. Carminati, Image formation in near field optics, *Prog. Surf. Sci.* **56**, 133 (1997).
- [38] N. Yamamoto, K. Araya, and F. J. García de Abajo, Photon emission from silver particles induced by a high-energy electron beam, *Phys. Rev. B* **64**, 205419 (2001).
- [39] F. J. García de Abajo and M. Kociak, Electron energy-gain spectroscopy, *New J. Phys.* **10**, 073035 (2008).
- [40] F. J. García de Abajo and M. Kociak, Probing the Photonic Local Density of States with Electron Energy Loss Spectroscopy, *Phys. Rev. Lett.* **100**, 106804 (2008).
- [41] F. J. García de Abajo, Optical excitations in electron microscopy, *Rev. Mod. Phys.* **82**, 209 (2010).
- [42] A. Losquin and M. Kociak, Link between cathodoluminescence and electron energy loss spectroscopy and the radiative and full electromagnetic local density of states, *ACS Photonics* **2**, 1619 (2015).
- [43] M. Cinchetti, A. Gloskovskii, S. A. Nepjiko, G. Schönhense, H. Rochholz, and M. Kreiter, Photoemission Electron Microscopy as a Tool for the Investigation of Optical Near Fields, *Phys. Rev. Lett.* **95**, 047601 (2005).
- [44] A. Kubo, K. Onda, H. Petek, Z. Sun, Y. S. Jung, and H. K. Kim, Femtosecond imaging of surface plasmon dynamics in a nanostructured silver film, *Nano Lett.* **5**, 1123 (2005).
- [45] A. Kubo, N. Pontius, and H. Petek, Femtosecond microscopy of surface plasmon polariton wave packet evolution at the silver/vacuum interface, *Nano Lett.* **7**, 470 (2007).
- [46] G. Spektor, D. Kilbane, A. K. Mahro, B. Frank, S. Ristok, L. Gal, P. Kahl, D. Podbiel, S. Mathias, H. Giessen, F.-J. M. zu Heringdorf, M. Orenstein, and M. Aeschlimann, Revealing the subfemtosecond dynamics of orbital angular momentum in nanoplasmonic vortices, *Science* **355**, 1187 (2017).
- [47] K. A. Willets and R. P. V. Duyne, Localized surface plasmon resonance spectroscopy and sensing, *Annu. Rev. Phys. Chem.* **58**, 267 (2007).
- [48] A. Campion and P. Kambhampati, Surface-enhanced Raman scattering, *Chem. Soc. Rev.* **27**, 241 (1998).
- [49] G. G. Paulus, W. Becker, W. Nicklich, and H. Walther, Rescattering effects in above-threshold ionization: a classical model, *J. Phys. B* **27**, L703 (1994).
- [50] P. Rácz, Z. Pápa, I. Márton, J. Budai, P. Wróbel, T. Stefaniuk, C. Prietl, J. R. Krenn, and P. Dombi, Measurement of nanoplasmonic field enhancement with ultrafast photoemission, *Nano Lett.* **17**, 1181 (2017).
- [51] J. Budai, Z. Pápa, I. Márton, P. Wróbel, T. Stefaniuk, Z. Márton, P. Rácz, and P. Dombi, Plasmon-plasmon coupling probed by ultrafast, strong-field photoemission with <7 Å sensitivity, *Nanoscale* **10**, 16261 (2018).
- [52] T. Paschen, C. Nauk, P. Dienstbier, and P. Hommelhoff, Strong-field spectra and optical near field enhancement at aluminium needle tips, *J. Phys. B* **54**, 144006 (2021).
- [53] S. Tojo, M. Hasuo, and T. Fujimoto, Absorption Enhancement of an Electric Quadrupole Transition of Cesium Atoms in an Evanescent Field, *Phys. Rev. Lett.* **92**, 053001 (2004).
- [54] R. Filter, S. Mühlig, T. Eichelkraut, C. Rockstuhl, and F. Lederer, Controlling the dynamics of quantum mechanical systems sustaining dipole-forbidden transitions via optical nanoantennas, *Phys. Rev. B* **86**, 035404 (2012).

- [55] M. Yamaguchi, K. Nobusada, T. Kawazoe, and T. Yatsui, Two-photon absorption induced by electric field gradient of optical near field and its application to photolithography, *Appl. Phys. Lett.* **106**, 191103 (2015).
- [56] M. Yamaguchi, K. Nobusada, and T. Yatsui, Nonlinear optical response induced by a second-harmonic electric-field component concomitant with optical near field excitation, *Phys. Rev. A* **92**, 043809 (2015).
- [57] M. Yamaguchi and K. Nobusada, Large hyperpolarizabilities of the second harmonic generation induced by nonuniform optical near fields, *J. Phys. Chem. C* **120**, 23748 (2016).
- [58] J. K. Sass, H. Neff, M. Moskovits, and S. Holloway, Electric field gradient effects on the spectroscopy of adsorbed molecules, *J. Phys. Chem.* **85**, 621 (1981).
- [59] H. D. Hallen, Nano-Raman spectroscopy: Surface plasmon emission, field gradients, and fundamentally near field propagation effects, *Nanobiotechnol.* **3**, 197 (2007).
- [60] Z. Zhang, M. Sun, P. Ruan, H. Zheng, and H. Xu, Electric field gradient quadrupole Raman modes observed in plasmon-driven catalytic reactions revealed by HV-TERS, *Nanoscale* **5**, 4151 (2013).
- [61] C. M. Aikens, L. R. Madison, and G. C. Schatz, The effect of field gradient on SERS, *Nat. Photonics* **7**, 508 (2013).
- [62] Y. Fang, Z. Zhang, L. Chen, and M. Sun, Near field plasmonic gradient effects on high vacuum tip-enhanced Raman spectroscopy, *Phys. Chem. Chem. Phys.* **17**, 783 (2015).
- [63] L. Meng, Z. Yang, J. Chen, and M. Sun, Effect of electric field gradient on sub-nanometer spatial resolution of tip-enhanced Raman spectroscopy, *Sci. Rep.* **5**, 9240 (2015).
- [64] L. Meng, Y. Wang, M. Gao, and M. Sun, Electromagnetic field gradient-enhanced Raman scattering in TERS configurations, *J. Phys. Chem. C* **125**, 5684 (2021).
- [65] W. Srituravanich, N. Fang, S. Durant, M. Ambati, C. Sun, and X. Zhang, Sub-100 nm lithography using ultrashort wavelength of surface plasmons, *J. Vac. Sci. Technol. B* **22**, 3475 (2004).
- [66] V. F. Dryakhlushin, A. Y. Klimov, V. V. Rogov, and N. V. Vostokov, Near-field optical lithography method for fabrication of the nanodimensional objects, *Appl. Surf. Sci.* **248**, 200 (2005).
- [67] E. Cefalí, S. Patané, and M. Lifshitz, Near-field optical lithography, in *Scanning Probe Microscopy in Nanoscience and Nanotechnology*, edited by B. Bhushan (Springer, Berlin, 2010), p. 757.
- [68] V. M. Murukeshan, K. V. Sreekanth, and J. K. Chua, Metal particle-surface system for plasmonic lithography, in *Lithography*, edited by M. Wang, (IntechOpen, London, 2010), Chap. 29.
- [69] A. Sarsa, F. Gálvez, and E. Buendía, Parameterized optimized effective potential for the ground state of the atoms He through Xe, *At. Data Nucl. Data Tables* **88**, 163 (2004).
- [70] J. A. Duncanson, Jr., M. P. Strand, A. Lindgard, and R. S. Berry, Angular Distributions of Electrons from Resonant Two-Photon Ionization of Sodium, *Phys. Rev. Lett.* **37**, 987 (1976).
- [71] C. Laughlin, One- and two-photon ionisation of the 3s and 3p states of Na I, *J. Phys. B* **11**, 1399 (1978).
- [72] A. Z. Msezane, W. Armstrong-Mensah, and J. Niles, Photoionization of Na: Resonance enhancement of the single-channel cross section, *Phys. Rev. A* **42**, 1286 (1990).
- [73] A. Bunjac, D. B. Popović, and N. S. Simonović, Calculations of photoelectron momentum distributions and energy spectra at strong-field multiphoton ionization of sodium, *Eur. Phys. J. D* **71**, 208 (2017).
- [74] V. P. Kosheleva, V. A. Zaytsev, R. A. Müller, A. Surzhykov, and S. Fritzsche, Resonant two-photon ionization of atoms by twisted and plane-wave light, *Phys. Rev. A* **102**, 063115 (2020).
- [75] Y. Boran, N. Hart, N. Kaya, J. Zhou, A. A. Kolomenskii, and H. A. Schuessler, Energy and angular distributions of electrons from sodium atoms photo-ionized with femtosecond laser pulses, *J. Phys. B* **54**, 145401 (2021).
- [76] A. Bunjac, D. B. Popović, and N. S. Simonović, On the selective multiphoton ionization of sodium by femtosecond laser pulses: A partial-wave analysis, *Phys. Lett. A* **394**, 127197 (2021).
- [77] Y. M. Amusia, *Atomic Photoeffect* (Plenum, New York, 1990).
- [78] J. W. Cooper, Photoionization from outer atomic subshells. a model study, *Phys. Rev.* **128**, 681 (1962).
- [79] I. Vartanyants, T.-L. Lee, S. Thiess, and J. Zegenhagen, Non-dipole effects in X-ray standing wave photoelectron spectroscopy experiments, *Nucl. Instrum. Methods Phys. Res., Sect. A* **547**, 196 (2005).
- [80] A. Gerlach, F. Schreiber, S. Sellner, H. Dosch, I. A. Vartanyants, B. C. C. Cowie, T.-L. Lee, and J. Zegenhagen, Adsorption-induced distortion of F₁₆CuPc on Cu(111) and Ag(111): An x-ray standing wave study, *Phys. Rev. B* **71**, 205425 (2005).
- [81] L. Landau and E. Lifshitz, *Quantum Mechanics: Non-Relativistic Theory*, 3rd ed., Course of Theoretical Physics (Pergamon, Oxford, 1991).